SCIENTIFIC REPORTS

OPEN

SUBJECT AREAS:
ATOMISTIC MODELS
CHEMICAL PHYSICS
STRUCTURE OF SOLIDS AND LIQUIDS

Received
1 October 2013

Accepted
31 October 2013

Published
20 November 2013

Correspondence and requests for materials should be addressed to J.Y.D. (jydai@nudt.edu.cn) or J.M.Y. (jmyuan@nudt.edu.cn)

# Quantum simulation of thermally-driven phase transition and oxygen *K*-edge x-ray absorption of high-pressure ice

Dongdong Kang[1], Jiayu Dai[1], Huayang Sun[1], Yong Hou[1] & Jianmin Yuan[1,2]

[1]Department of Physics, College of Science, National University of Defense Technology, Changsha 410073, Hunan, People's Republic of China, [2]State Key Laboratory of High Performance Computing, National University of Defense Technology, Changsha 410073, Hunan, People's Republic of China.

**The structure and phase transition of high-pressure ice are of long-standing interest and challenge, and there is still a huge gap between theoretical and experimental understanding. The quantum nature of protons such as delocalization, quantum tunneling and zero-point motion is crucial to the comprehension of the properties of high-pressure ice. Here we investigated the temperature-induced phase transition and oxygen *K*-edge x-ray absorption spectra of ice VII, VIII and X using *ab initio* path-integral molecular dynamics simulations. The tremendous difference between experiments and the previous theoretical predictions is closed for the phase diagram of ice below 300 K at pressures up to 110 GPa. Proton tunneling assists the proton-ordered ice VIII to transform into proton-disordered ice VII where only thermal activated proton-transfer cannot occur. The oxygen *K* edge with its shift is sensitive to the order-disorder transition, and therefore can be applied to diagnose the dynamics of ice structures.**

Ice is of great scientific interest due to its fundamental significance in many fields, such as biology, chemistry, astrophysics and environmental science. As the most important prototype of hydrogen bond (HB), understanding the properties of water and ice over a wide range of temperature and pressure are still interesting and challenging[1,2]. Furthermore, the knowledge of compressed ice is essential for modeling the interiors and evolutions of solar planets (e.g., Uranus and Neptune) and exoplanets[3,4]. Therefore, a lot of efforts have been made to explore the structures and peculiar properties of ice in both experiments and theoretical calculations[5]. To date, at least 16 crystalline phases of ice have been identified experimentally[6], and new ultrahigh-pressure phases are continually predicted theoretically[7–9]. These phases compose a fairly complicated phase diagram of ice.

Among the rich phases of ice, three phases, ice VII, VIII, and X, occupy a large region of the phase diagram above 2 GPa. Compared with the proton-disordered structure of ice VII, ice VIII is proton ordered and antiferroelectric due to the dipole moments associated with water molecules on the two sublattices pointing in opposite directions[10]. With increasing pressure, both ice VII and VIII transform into a symmetric HB phase, ice X, in which the protons are located at the middle between two neighbouring oxygen atoms[11,12]. The phase transitions among these phases of dense ice have been extensively studied from experiments. The infrared absorption[13] and x-ray diffraction[14] measurements have evidenced that the VII-VIII boundary remains at 273 K up to 12 GPa and then rapidly decreases toward 0 K at approximately 60 GPa. Unfortunately, there is a great gap between theoretical results and experimental data for this phase boundary, although the trend is qualitatively reproduced in *ab initio* calculations[15].

Due to their low mass, quantum nature of protons involving quantum tunneling and zero-point motion (ZPM) is crucial to structures of water[16,17] and ice[18–20] as well as other light-atom systems[21–23]. For instance, nuclear quantum effects (NQEs) could considerably soften the structure of the liquid water[16] and contribute the anomalously high mobility of hydrated excess proton in water[17]. Moreover, the calculated proton momentum distribution in high-pressure ice can be greatly improved with the inclusion of NQEs[18]. In particular, the quantum simulations treating protons as quantum particles have showed that quantum tunneling induces the proton order-disorder transition of ice VII, VIII and X[19,20]. Therefore, in order to obtain the exact phase diagram of ice at finite temperatures from theoretical calculation, NQEs need to be properly taken into account. More importantly, it should be noted that the thermal effects induced by temperature and NQEs jointly determine the phase transitions between these high-pressure phases. However, the thermally-driven phase transitions of

high-pressure ice are rarely investigated theoretically. The current experimental probes for phase transitions of high-pressure ice such as x-ray diffraction, infrared and Raman spectra involve only the ionic structure and lack the information about electronic structure. Core-level spectroscopy has been shown to be an important probe of investigating the microscopic structure of complex materials from the level of electronic structure[24,25]. Many x-ray absorption near-edge spectroscopy (XANES) measurements and theoretical calculations have been successfully applied to water and ice at ambient conditions[26–29]. These results showed that the oxygen *K*-edge XANES is surprisingly sensitive to the bonding situation in HB network. However, it is a great theoretical challenge to reproduce the measured XANES and connect XANES with microscopic structure of materials. As reported by Kong *et al.*[30], NQEs strongly affect the XANES of water and ice $I_h$. Therefore, for high-pressure ice it is expected that the quantum treatment of protons in theoretical calculations is indispensable to XANES.

In the present work, we use *ab initio* path-integral molecular dynamics[31] (PIMD) to highlight the significance of NQEs on phase transition and *K*-edge XANES of ice VII, VIII and X at temperatures below 300 K. The results show that the calculations including NQEs almost close the gap between theoretical and experimental results for phase diagram of ice VII, VIII and X. Moreover, the *K*-edge XANES is sensitive to the order-disorder transition between ice VIII and VII, thus can be applied to characterize the phase transition of ice.

## Results

**Thermally-driven phase transition of high-pressure ice.** In order to gain thorough insight into the phase transitions between ice VII, VIII, and X, we performed *ab initio* PIMD simulations for three representative cubic box sizes of 5.82 Å, 5.56 Å, and 5.34 Å at three temperatures of 100 K, 200 K, and 300 K. The corresponding pressures for the three cells are 34.5 GPa, 61.2 GPa and 107.9 GPa, respectively. The increase of pressure induced by temperature rising from 100 K to 300 K is within 0.8 GPa.

Firstly, we simulated the proton behavior at 34.5 GPa with increasing temperature. Comparisons of the average proton distributions as a function of the proton-transfer coordinate $\delta$ and the corresponding oxygen-oxygen separation $d_{OO}$ between classical and quantum simulations are presented in Fig. 1. The proton-transfer coordinate $\delta$ is defined as the difference between two instantaneous O-H distances. When $\delta = 0$, the proton is located midway between its two nearest neighbouring oxygen atoms. We can see from Fig. 1 that NQEs have a significant impact on the proton transfer. At 100 K, both classical and quantum simulations exhibit proton-ordered structure, corresponding to ice VIII, although the quantum simulation shows more delocalized character than classical simulation.

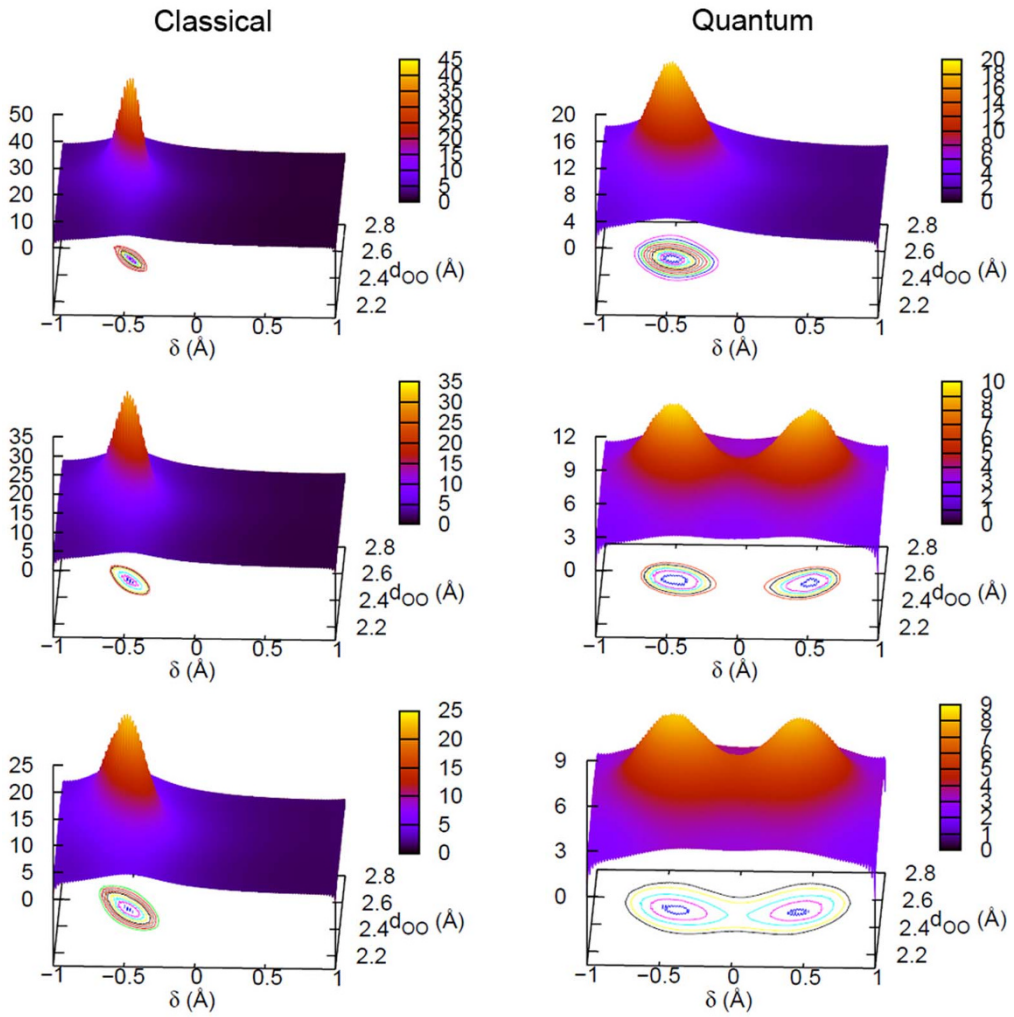


**Figure 1 | The average proton distribution function $P(\delta, d_{OO})$ as a function of the proton position relative to the bond midpoint $\delta$ and the corresponding oxygen-oxygen separation $d_{OO}$ in classical (left panels) and quantum (right panels) simulations at 34.5 GPa.** The corresponding temperature is 100 K, 200 K and 300 K from top to bottom.

When the temperature is increased to 200 K, the protons distribute with a bimodal structure with the inclusion of NQEs. It means that the protons tunnel through the potential barrier between two equivalent sites along their two nearest neighbouring oxygen atoms and exhibit disordered structure. Here ice has transformed from VIII to VII, which is in good agreement with the experimental measurements[13]. On the contrary, this phase transition cannot be reproduced by classical simulations. Even at 300 K, ice is still in VIII phase in classical simulations (see Fig. 1). It indicates that the ice VIII-VII transition is dominated by nuclear quantum tunneling rather than thermal fluctuation.

The average proton distributions at 61.2 GPa are shown in Fig. 2. We can see that at 100 K the proton distributions exhibit a greatly reduced bimodal structure in quantum simulation, but the unimodal structure in classical simulation. The two types of proton distribution correspond to VII and VIII phase, respectively. Above 200 K, on one hand, thermal hopping appears in classical simulation, which does not occur at low pressure of 34.5 GPa. It is due to the fact that the potential barrier along the neighbouring oxygen atoms is greatly suppressed under compression and thermal fluctuation could assist protons to turn over the potential barrier and transfer between two equal sites along the HB. On the other hand, when NQEs are taken into account, the protons exhibit a considerably broadened unimodal distribution, which arises from the nuclear quantum delocalization. Our simulations show that under a compression of 61.2 GPa ice is in phase VII at 100 K and phase X at 200 K and 300 K, which is consistent with the infrared measurements[13].

We note previous simulations[20] and x-ray diffraction measurements[14] suggested that ice X undergoes a dynamically disordered structure before transforming to the fully centered X. In the dynamically disordered ice X, the protons occupy the two stable sites along the HB with a very low potential barrier. In our PIMD simulations, there exists a much broad and flat but unimodal peak of proton distributions at 61.2 GPa above 200 K, which indicates that the protons vibrate over a broad region between their two neighbouring oxygen atoms. The character of the dynamically disordered ice X does not exhibit obviously here. At 107.9 GPa, both classical and quantum simulations display unimodal structure of the average proton distributions from 100 K to 300 K and the peaks become much sharper and the proton becomes more localized than those at 61.2 GPa (see Supplementary Fig. S1). At 107.9 GPa, ice is in symmetric HB phase X. It should be stressed that these features involving phase transitions of ice VIII, VII and X are greatly determined by NQEs and cannot be illustrated by classical simulations.

The phase transitions between ice VII, VIII and X can be characterized by the changes of O-H bonding, which is expected to be dramatically influenced under compression. In order to clarify the changes of O-H bonding in high-pressure ice, we show the distributions of the O-H bond lengths at different pressures and temperatures in Fig. 3a. Firstly, we note that compression shortens the HB

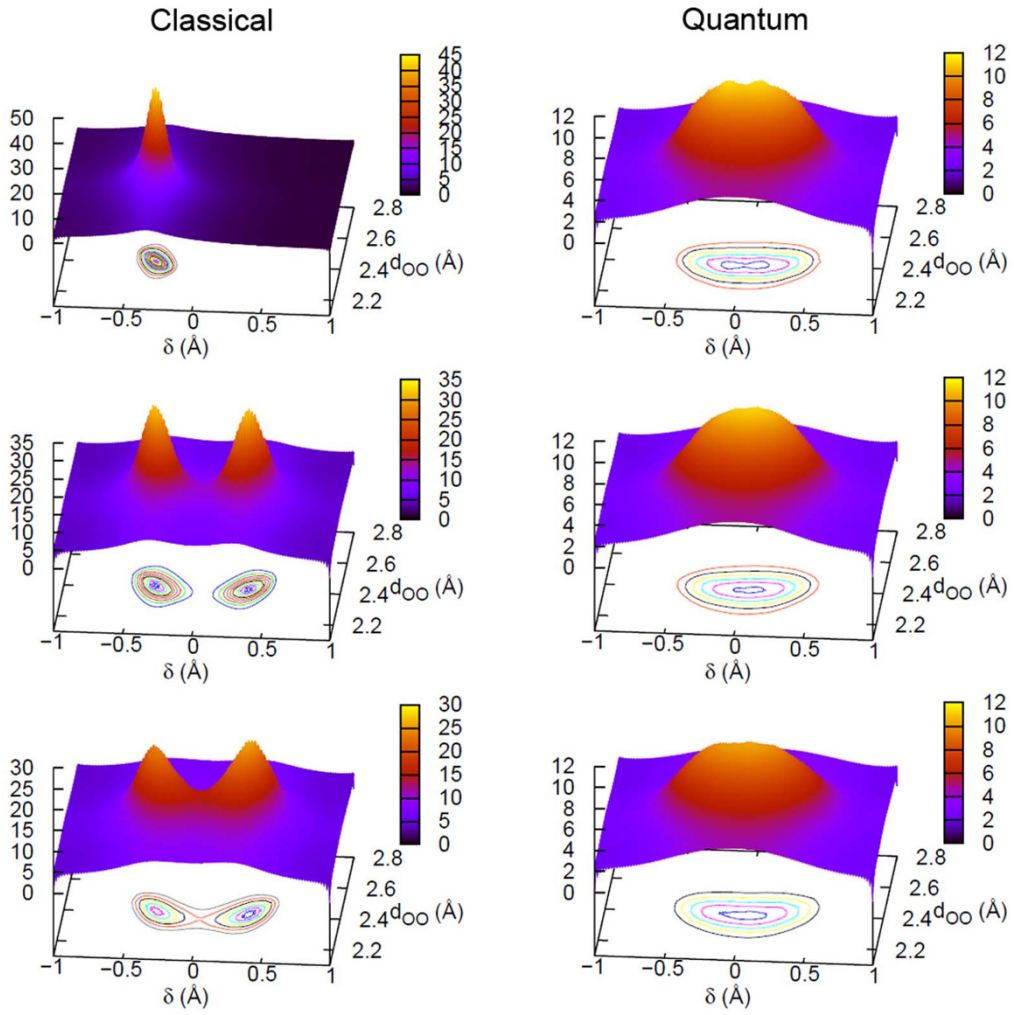


**Figure 2 | The average proton distribution function $P(\delta,d_{OO})$ as a function of the proton position relative to the bond midpoint $\delta$ and the corresponding oxygen-oxygen separation $d_{OO}$ in classical (left panels) and quantum (right panels) simulations at 61.2 GPa.** The corresponding temperature is 100 K, 200 K and 300 K from top to bottom.

and lengthens the covalent O-H bond both in classical and quantum simulations, which is in agreement with the recent reports[1,2]. In the classical simulations, two distinct peaks at 34.5 GPa represent the short covalent bond and long HB, respectively, and are still fully separated even up to 300 K. They start to merge together at 61.2 GPa and 200 K and finally become one sharp peak when the pressure is increased to 107.9 GPa. When NQEs are taken into account, since the protons can tunnel through the potential barrier along two nearest neighbouring oxygen atoms, the strong covalent O-H bond can transform into weak HB at 34.5 GPa and 200 K. Furthermore, the distinction between the covalent bond and HB at 61.2 GPa becomes almost disappeared, and two sharp peaks are replaced by a broad and reduced peak above 200 K. It indicates that ice is in symmetric HB phase X above 200 K at the pressure of 61.2 GPa. The sharp peaks of the distributions of the O-H bond lengths at 107.9 GPa indicate the protons occupy the midpoint between neighbouring oxygen atoms with localized vibrations and the O-H bonds are completely symmetric HB under these conditions.

Corresponding to the distributions of proton shown in Fig. 1 and 2, the free energy profiles[22] $\Delta F$ as a function of proton-transfer coordinate $\delta$ are presented in Fig. 3b. The free energy profile is defined as $\Delta F = -k_B T \ln[P(\delta)]$, where $P(\delta)$ is the probability distribution of $\delta$ and $k_B$ is the Boltzmann constant. It can be seen from Fig. 3b that NQEs induce a dramatic influence on the free energy profiles. We note that ice VIII is proton ordered while ice VII is proton-disordered. As a result, the free energy profiles exhibit a single-well structure for ice VIII and double-well structure for ice VII. This character is reproduced only when the nuclear quantum feature is considered. In particular, the proton-ordered ice VIII transforms to proton-disordered ice VII through thermal hopping at 61.2 GPa and 200 K in the classical simulations, nevertheless, ice has transformed from VII to symmetric phase X under the same condition when NQEs are considered.

In order to obtain the phase diagram of high-pressure ice, we choose five pressure points for phase boundary between ice VII and VIII and three temperature points for transformation from ice VII and VIII into X. For phase boundary between ice VII and VIII, the simulations were performed at every 25 K, while for transformation to ice X, the size of cubic cell was changed with 0.5 a.u.. The occurrence of proton transfer is considered as the criterion of phase transition from ice VIII to VII. The transformation from bimodal to unimodal structure of average proton distribution indicates that either ice VII or VIII has transformed into X. According to these criteria, the phase diagram of ice determined from the PIMD calculations is shown in Fig. 4. Many experimental data[12,13,32–34] involving infrared and Raman spectra and theoretical results reported by Umemoto *et al.*[15] are also displayed for comparison. The transition temperature between ice VII and VIII in Ref. 15 was obtained from the peak of the constant pressure heat capacity. We can see that the transition temperature obtained from static calculations in Ref. 15 is greatly lower than experimental data, and even with the inclusion of vibrational contributions through quasi-harmonic approximation, the phase boundary between ice VII and VIII is not improved. It is mainly attributed to the absence of nuclear quantum tunneling in their calculations. In our calculations, we properly described the NQEs including quantum tunneling and ZPM via PIMD. The phase boundaries between ice VII, VIII and X exhibit the same behavior as experimental data[13]. Furthermore, the transition temperature and transition pressure from our results are in good agreement with experimental data[13], although the transition temperature between ice VII and VIII is lower than experimental data by about 30 K and the transition pressure between ice VII and X is lower than experimental data by about 5 GPa. Actually, in classical simulations the transition temperatures between ice VII and VIII is much higher than the experimental results and the transition pressures from ice VII and VIII into X are also much larger than the experimental results. When taking into account NQEs, the greatly improved phase diagram of ice below 300 K at pressures up to 110 GPa is obtained (Note that the region of 90–110 GPa of phase X is not shown in Fig. 4).

***K*-edge x-ray absorption of high-pressure ice.** As the complementary probe of microscopic structure in high-pressure ice, oxygen *K*-edge XANES is calculated based on DFT with Perdew-Burke-Ernzerhof[35] (PBE) exchange-correlation potential. We note that an accurate electronic structure is required to obtain reliable optical spectra. Thus the Heyd-Scuseria-Ernzerhof[36] (HSE) hybrid functional is employed to compare with the PBE functional. We calculated XANES spectra of one configuration randomly extracted from the molecular dynamics (MD) simulations with HSE and PBE functional and the result indicated that HSE hybrid functional has a slightly influence on the XANES and PBE functional could obtain reliable results for high-pressure ice.

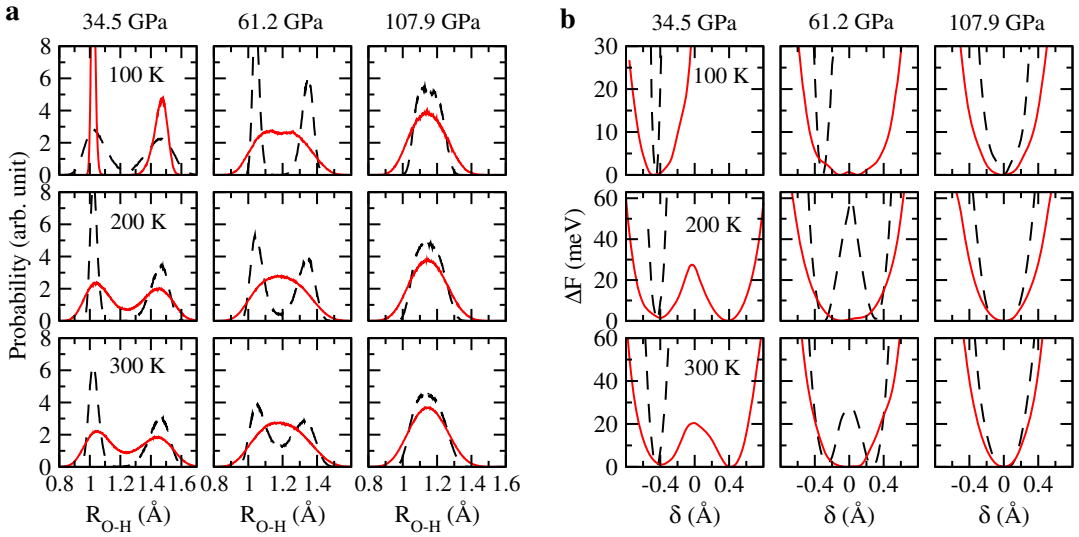


**Figure 3** | (a) Distributions of the O-H bond lengths at different pressures and temperatures and (b) free energy profiles of the protons along the two nearest neighbouring oxygen atoms obtained from quantum (solid lines) and classical (dashed lines) simulations. The pressure is from 34.5 GPa (left), 61.2 GPa (middle) to 107.9 GPa (right) and the temperature is increased from 100 K (top), 200 K (middle) to 300 K (bottom).

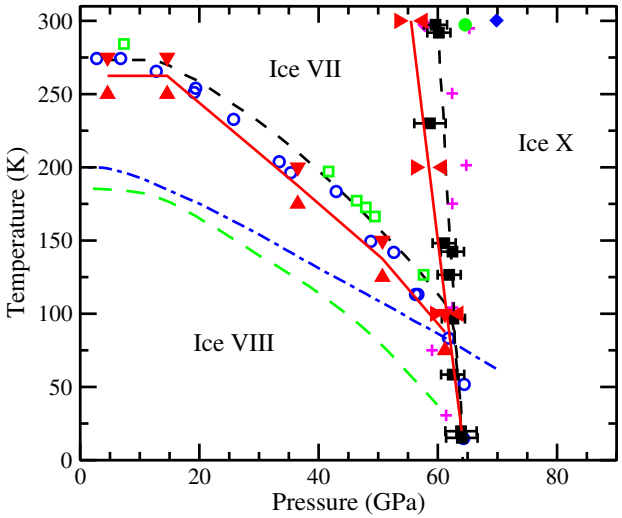


**Figure 4 | Phase diagram of ice VII, VIII and X below 300 K. The red solid lines are the phase boundary between ice VII, VIII and X obtained from our calculations.** The solid up triangles and down triangles denote the lower and upper bound of the phase boundary between ice VII and VIII, respectively. The solid right triangles and left triangles denote the left and right bound of the phase transition between ice X and the other two phases. The green dashed line and blue dot-dashed line are from theoretical results in Ref. 15. The experimental data previously reported are presented by black dashed lines and solid squares (Ref. 13), open circles (Ref. 12), open squares and crosses (Ref. 32), a solid circle (Ref. 33) and a solid diamond (Ref. 34).

For comparison with the experimental data, the XANES of ice VIII at 2.2 GPa at 250 K are calculated. The experiment is the x-ray Raman scattering[37] which is equivalent to XANES in the limit of small momentum transfer. Comparisons of XANES between theoretical calculations and experiment shown in Fig. 5a indicate that the classical simulation overestimates the pre-edge at about 535 eV and underestimates the post-edge above 540 eV. When the NQEs are taken into account, the spectrum is substantially improved and reaches better agreement with experiment. However, there still exist slight deviations in main edge and post-edge regions from experiment. These deviations may be due to the single-particle approximation in DFT, which ignores the many-body effects of electrons.

The XANES of ice VIII, VII and X with increasing pressure at 100 K are shown in Fig. 5b–5d. One obvious feature is that the pre-edge is reduced with increasing pressure. Ice VIII exhibits visible pre-edge (see Fig. 5a and 5b) whereas ice VII and X do not have this stage (see Fig. 5c and 5d). A lot of previous studies on oxygen *K*-edge XANES of water and ice have shown that the pre-edge is sensitive to the local HB environment[26–28], that is to say, the breaking of HB could enhances the pre-edge intensity, on the contrary, the strengthening of HB would reduce the pre-edge. In our quantum simulations, the reduced pre-edge of ice VIII from 2.2 GPa to 34.5 GPa can be attributed to the shortened distances between oxygen atoms under compression, thereby enhancing the HB. Furthermore, the pre-edge disappears when the proton-ordered ice VIII transforms to the proton-disordered ice VII and symmetric HB ice X. It indicates that the order-disorder transition of high-pressure ice can be characterized by the pre-edge of oxygen *K*-edge spectra. However, the main edge and post-edge are insensitive to the order-disorder transition, as shown in Fig. 5. In addition, the increasing differences of the XANES between classical and quantum simulations with pressure arise from the enhanced NQEs at high pressures. The differences are reduced with increasing temperature (see Supplementary Fig. S2).

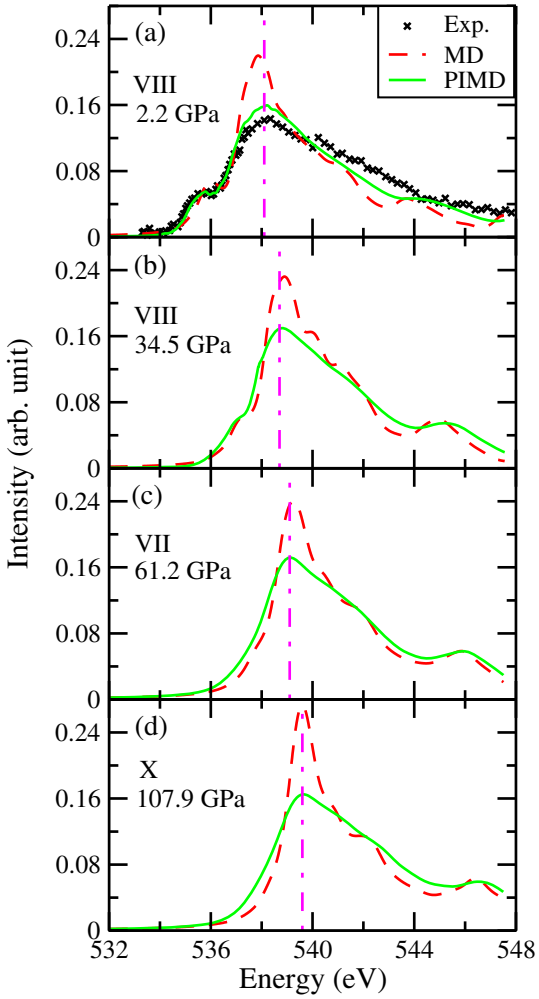


**Figure 5 | Comparisons of calculated XANES spectra obtained from quantum (solid lines) and classical simulations (dashed lines).** The experiment result for ice VIII at 2.2 GPa is from Ref. 37. The temperature is 250 K for ice VIII at 2.2 GPa (a) and 100 K for the other three cases. The calculated results in (a) are aligned at the onset and normalized to the same area for comparison with experiment. The results in (b)–(d) are shifted with the same value as (a) for comparisons. The dot-dashed lines denote the peak position of PIMD results. The shift of peak position is 0.6 eV, 1.0 eV and 1.5 eV for (b), (c) and (d) compared with (a).

The features of XANES originate essentially from the electronic structure. The electronic density of states (DOS) corresponding to the XANES is illustrated in Fig. 6. For convenience, we set the top of the valence bands as the Fermi level. It can be clearly seen that NQEs induce a strong impact on the electronic properties, as pointed out by Cannuccia *et al.*[38]. In particular, all the bands are greatly broadened when NQEs are considered via PIMD, which correspond to the broadened XANES in quantum simulations. Interestingly, we note that the band gap is increased with pressure, corresponding to the shift of peak position of XANES (see Fig. 5). Indeed, when atoms in ice become closer under compression, the overlap of electronic wave functions makes energy levels not only broadened but also shift to higher value. Moreover, the conduct bands shift much faster than the valence bands[39], thereby inducing the increased band gap.

## Discussion

In this work, we have performed *ab initio* PIMD simulations for ice VII, VIII and X at temperatures of 100 K, 200 K to 300 K as well as their classical counterparts. The results showed that NQEs play a

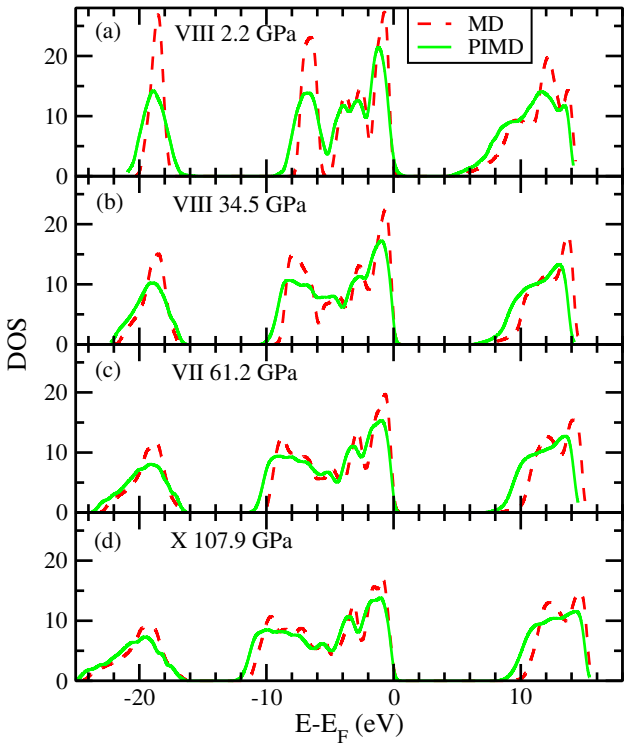


**Figure 6 | Comparisons of electronic density of states (DOS) calculated from quantum (solid lines) and classical simulations (dashed lines).** The temperature is 250 K for ice VIII at 2.2 GPa (a) and 100 K for the other three cases.

crucial role in the phase transitions between ice VII, VIII and X. Proton tunneling assists the proton-ordered ice VIII to transform into proton-disordered ice VII. When the pressure is increased up to 61.2 GPa, the molecular phase VII transforms to the atomic phase X above 200 K. At 107.9 GPa, the protons are fully centered at the midpoint between their neighboring oxygen atoms. Our results are in good agreement with experimental results. Moreover, NQEs induce strong impact on the oxygen *K*-edge XANES in high-pressure ice. Greatly broadened XANES originate from the broadened DOS with the inclusion of NQEs. For ice VIII, the pre-edge of oxygen *K* edge is reduced from 2.2 GPa to 34.5 GPa due to the enhancement of HB, and then disappears when transforming to ice VII, which is the result of order-disorder transition between ice VIII and VII. Despite these improvements of theoretical results, we note that there are still small deviations between theoretical calculations and experiments, which are expected to be improved with more accurate calculations of electronic structure, including accurate van der Waals and many-electron correlation.

## Methods

In *ab initio* path-integral molecular dynamics (PIMD) calculations, the nuclei were quantized using Feynman's path-integral representation of quantum statistical mechanics, while the electronic structure was described by density functional theory (DFT). All PIMD calculations as well as their classical counterparts in this work were performed with modified Quantum-ESPRESSO package[21,40] based on DFT.

Electronic structure calculations were carried out based on pseudopotential with plane-wave expansion of electronic wave functions. The Perdew-Burke-Ernzerhof generalized-gradient approximation[35] was employed for exchange-correlation potential. The ultrasoft pseudopotential was used to describe the interaction between valence and core electrons. After careful tests, a plane-wave energy cutoff of 50 Ry was adopted with the charge-density cutoff of 400 Ry. An empirical dispersion correction is adopted to treat van der Waals interaction[41]. A cubic supercell including 16 water molecules subject to periodic boundary conditions was employed. Larger supercell including up to 64 water molecules was employed to test convergence of cell size and the results showed no influence on the phase boundary between ice VII, VIII and X. The lattice of ice VIII is not cubic cell but tetragonally distorted slightly[10]. Although the cubic lattice for ice VIII in our simulations could induce slight error, the physics can be captured[19]. The $\Gamma$ point was used for sampling the Brillouin zone when performing molecular dynamics simulations. A $2 \times 2 \times 2$ k-points grid was used to calculate the pressure when considering the phase boundary. After careful tests, the difference of pressure with more dense k-points grid is within 1 GPa.

The primitive discretization of the path-integral formalism with staging transformation was used for static sampling of the imaginary time paths[31]. Langevin thermostat[42] was employed to overcome the nonergodic problem, which not only produces a canonical ensemble and compensates the calculated errors, and has been proved efficiently under extreme conditions[43,44]. The path integral was discretized using $P = 16$ Trotter replicas. The fictitious sampling masses are set to be 4 times larger than the corresponding physical masses of the nuclei. Time step of 8 a.u. was used in our simulations. After an equilibration of 3.5 ps, a total of 40000 configurations were generated for three ice phases, respectively. Randomly sampled ice configuration after equilibration was used to be the starting configuration for PIMD simulations.

For the calculations of x-ray absorption near-edge spectroscopy (XANES), DFT based *ab initio* approach is computationally efficient and could give satisfactory results[26,29,45]. In our calculations, oxygen *K*-edge XANES was obtained based on DFT using Fermi's golden rule with the final state of the electronic system in the presence of the core hole to mimic the x-ray excitation[40,46]. The supercell including 16 water molecules was employed to obtain XANES. Larger supercell including up to 64 water molecules was adopted to test convergence of cell size and the results showed that the size of 16 water molecules is big enough for obtaining reliable XANES (see Supplementary Fig. S3). A oxygen pseudopotential with one electron removed from the 1 s orbital was used. We adopted a $4 \times 4 \times 4$ k-points grid and a 90 Ry plane-wave energy cutoff to ensure the convergence. The calculated spectra were broadened using a Gaussian convolution of width 0.3 eV. We extracted 10 independent snapshots from molecular dynamics simulations at each temperature-pressure state, then for each snapshot, the XANES spectra are averaged from each oxygen atom. In the PIMD calculations, the spectra are also averaged from the imaginary time replicas.


1. Huang, Y. *et al.* Size, separation, structural order, and mass density of molecules packing in water and ice. *Sci. Rep.* **3**, 3005; DOI:10.1038/srep03005 (2013).
2. Huang, Y. *et al.* Hydrogen bond asymmetric local potentials in compressed ice. *J. Phys. Chem. B* DOI:10.1021/jp407836n (2013).
3. Guillot, T. Interiors of giant planets inside and outside the solar system. *Science* **286**, 72–77 (1999).
4. Lissauer, J. J. Extrasolar planets. *Nature* **419**, 355–358 (2002).
5. Malenkov, G. Liquid water and ices: Understanding the structure and physical properties. *J. Phys.: Condens. Matter* **21**, 283101 (2009).
6. Salzmann, C. G., Radaelli, P. G., Mayer, E. & Finney, J. L. Ice XV: A new thermodynamically stable phase of ice. *Phys. Rev. Lett.* **103**, 105701 (2009).
7. Wang, Y. *et al.* High pressure partially ionic phase of water ice. *Nat. Commun.* **2**, 563–567 (2011).
8. McMahon, J. M. Ground-state structures of ice at high pressures from ab initio random structure searching. *Phys. Rev. B* **84**, 220104(R) (2011).
9. Ji, M., Umemoto, K., Wang, C.-Z., Ho, K.-M. & Wentzcovitch, R. M. Ultrahigh-pressure phases of H2O ice predicted using an adaptive genetic algorithm. *Phys. Rev. B* **84**, 220105(R) (2011).
10. Kuo, J.-L. & Klein, M. L. Structure of Ice-VII and Ice-VIII: A quantum mechanical study. *J. Phys. Chem. B* **108**, 19634–19639 (2004).
11. Holzapfel, W. B. On the symmetry of hydrogen bonds in ice VII. *J. Chem. Phys.* **56**, 712–715 (1972).
12. Pruzan, Ph., Chervin, J. C. & Canny, B. Stability domain of the ice VIII proton-ordered phase at very high pressure and low temperature. *J. Chem. Phys.* **99**, 9842–9846 (1993).
13. Song, M., Yamawaki, H., Fujihisa, H., Sakashita, M. & Aoki, K. Infrared investigation on ice VIII and the phase diagram of dense ices. *Phys. Rev. B* **68**, 014106 (2003).
14. Sugimura, E. *et al.* Compression of H2O ice to 126 GPa and implications for hydrogen-bond symmetrization: Synchrotron x-ray diffraction measurements and density-functional calculations. *Phys. Rev. B* **77**, 214103 (2008).
15. Umemoto, K., Wentzcovitch, R. M., de Gironcoli, S. & Baroni, S. Order–disorder phase boundary between ice VII and VIII obtained by first principles. *Chem. Phys. Lett.* **499**, 236–240 (2010).
16. Morrone, J. A. & Car, R. Nuclear quantum effects in water. *Phys. Rev. Lett.* **101**, 017801 (2008).
17. Marx, D., Tuckerman, M. E., Hutter, J. & Parrinello, M. The nature of the hydrated excess proton in water. *Nature* **397**, 601–604 (1999).
18. Morrone, J. A., Lin, L. & Car, R. Tunneling and delocalization effects in hydrogen bonded systems: A study in position and momentum space. *J. Chem. Phys.* **130**, 204511 (2009).
19. Benoit, M., Marx, D. & Parrinello, M. Tunneling and zero-point motion in high-pressure ice. *Nature* **392**, 258–261 (1998).
20. Benoit, M., Romero, A. H. & Marx, D. Reassigning hydrogen-bond centering in dense ice. *Phys. Rev. Lett.* **89**, 145501 (2002).
21. Kang, D. *et al.* Revealing the Complex Transport Behaviors in Warm Dense Hydrogen by Including Nuclear Quantum Effects. *arXiv*:1304.0953 (2013).
22. Li, X.-Z., Probert, M. I. J., Alavi, A. & Michaelides, A. Quantum nature of the proton in water-hydroxyl overlayers on metal surfaces. *Phys. Rev. Lett.* **104**, 066102 (2010).

23. Li, X.-Z., Walker, B. & Michaelides, A. Quantum nature of the hydrogen bond. *Proc. Natl. Acad. Sci. U.S.A.* **108**, 6369–6373 (2011).
24. Tanaka, I. & Mizoguchi, T. First-principles calculations of x-ray absorption near edge structure and energy loss near edge structure: present and future. *J. Phys.: Condens. Matter* **21**, 104201 (2009).
25. Zeng, J. & Yuan, J. Detailed-term-accounting approximation calculations of the radiative opacity of aluminum plasmas: A systematic study. *Phys. Rev. E* **66**, 016401 (2002).
26. Hetényi, B., De Angelis, F., Giannozzi, P. & Car, R. Calculation of near-edge x-ray-absorption fine structure at finite temperatures: Spectral signatures of hydrogen bond breaking in liquid water. *J. Chem. Phys.* **120**, 8632–8637 (2004).
27. Chen, W., Wu, X. & Car, R. X-ray absorption signatures of the molecular environment in water and ice. *Phys. Rev. Lett.* **105**, 017802 (2010).
28. Zhang, J., Xiao, Z.-R. & Kuo, J.-L. Calculation of near K edge x-ray absorption spectra and hydrogen bond network in ice XIII under compression. *J. Chem. Phys.* **132**, 184506 (2010).
29. Vinson, J., Kas, J. J., Vila, F. D., Rehr, J. J. & Shirley, E. L. Theoretical optical and x-ray spectra of liquid and solid H2O. *Phys. Rev. B* **85**, 045101 (2012).
30. Kong, L., Wu, X. & Car, R. Roles of quantum nuclei and inhomogeneous screening in the x-ray absorption spectra of water and ice. *Phys. Rev. B* **86**, 134203 (2012).
31. Marx, D. & Parrinello, M. Ab initio path integral molecular dynamics: Basic ideas. *J. Chem. Phys.* **104**, 4077–4082 (1996).
32. Goncharov, A. F., Struzhkin, V. V., Mao, H.-K. & Hemley, R. J. Raman spectroscopy of dense H2O and the transition to symmetric hydrogen bonds. *Phys. Rev. Lett.* **83**, 1998–2001 (1999).
33. Aoki, K., Yamawaki, H., Sakashita, M. & Fujihisa, H. Infrared absorption study of the hydrogen-bond symmetrization in ice to 110 GPa. *Phys. Rev. B* **54**, 15673–15677 (1996).
34. Struzhkin, V. V., Goncharov, A. F., Hemley, R. J. & Mao, H.-K. Cascading Fermi resonances and the soft mode in dense ice. *Phys. Rev. Lett.* **78**, 4446–4449 (1997).
35. Perdew, J. P., Burke, K. & Ernzerhof, M. Generalized gradient approximation made simple. *Phys. Rev. Lett.* **77**, 3865–3868 (1996).
36. Heyd, J., Scuseria, G. E. & Ernzerhof, M. Hybrid functionals based on a screened Coulomb potential. *J. Chem. Phys.* **118**, 8207–8215 (2003).
37. Pylkkänen, T. *et al.* Role of non-hydrogen-bonded molecules in the oxygen K-edge spectrum of ice. *J. Phys. Chem. B* **114**, 3804–3808 (2010).
38. Cannuccia, E. & Marini, A. Effect of the quantum zero-point atomic motion on the optical and electronic properties of diamond and trans-polyacetylene. *Phys. Rev. Lett.* **107**, 255501 (2011).
39. Hou, Y., Jin, F. & Yuan, J. Influence of the electronic energy level broadening on the ionization of atoms in hot and dense plasmas: An average atom model demonstration. *Phys. Plasmas* **13**, 093301 (2006).
40. Giannozzi, P., Baroni, S., Bonini, N., Calandra, M., Car, R., Cavazzoni, C., Ceresoli, D., Chiarotti, G. L., Cococcioni, M., Dabo, I., Corso, A. D., de Gironcoli, S., Fabris, S., Fratesi, G., Gebauer, R., Gerstmann, U., Gougoussis, C., Kokalj, A., Lazzeri, M., Martin-Samos, L., Marzari, N., Mauri, F., Mazzarello, R., Paolini, S., Pasquarello, A., Paulatto, L., Sbraccia, C., Scandolo, S., Sclauzero, G., Seitsonen, A. P., Smogunov, A., Umari, P. & Wentzcovitch, R. M. QUANTUM ESPRESSO: a modular and open-source software project for quantum simulations of materials. *J. Phys.: Condens. Matter* **21**, 395502 (2009).
41. Grimme, S. Semiempirical GGA-type density functional constructed with a long-range dispersion correction. *J. Comput. Chem.* **27**, 1787–1799 (2006).
42. Kühne, T. D., Krack, M., Mohamed, F. R. & Parrienllo, M. Efficient and accurate Car-Parrinello-like approach to Born-Oppenheimer molecular dynamics. *Phys. Rev. Lett.* **98**, 066401 (2007).
43. Dai, J., Hou, Y. & Yuan, J. Unified first principles description from warm dense matter to ideal ionized gas plasma: Electron-ion collisions induced friction. *Phys. Rev. Lett.* **104**, 245001 (2010).
44. Dai, J., Kang, D., Zhao, Z., Wu, Y. & Yuan, J. Dynamic ionic clusters with flowing electron bubbles from warm to hot dense iron along the Hugoniot curve. *Phys. Rev. Lett.* **109**, 175701 (2012).
45. Schwartz, C. P., Uejio, J. S., Saykally, R. J. & Prendergast, D. On the importance of nuclear quantum motions in near edge x-ray absorption fine structure spectroscopy of molecules. *J. Chem. Phys.* **130**, 184109 (2009).
46. Gougoussis, C., Calandra, M., Seitsonen, A. P. & Mauri, F. First-principles calculations of x-ray absorption in a scheme based on ultrasoft pseudopotentials: From a-quartz to high-Tc compounds. *Phys. Rev. B* **80**, 075102 (2009).


## Acknowledgments

This work is supported by the National Basic Research Program of China (973 Program) under Grant No. 2013CB922203, the National Natural Science Foundation of China under Grant Nos. 11104351, 11274383 and 11005153. D.K. thanks the support of the Hunan Provincial Innovation Foundation for Postgraduate under Grant No. CX2011B009. Calculations were carried out at the Research Center of Supercomputing Application, NUDT.

## Author contributions

D.K., J.D. and J.Y. designed the research. D.K. and J.D. modified the code. D.K. performed all calculations. D.K., J.D., H.S. and Y.H. analysed the data. D.K., J.D. and J.Y. wrote the paper. All authors reviewed the manuscript.

## Additional information

**Supplementary information** accompanies this paper at http://www.nature.com/scientificreports

**Competing financial interests:** The authors declare no competing financial interests.

**How to cite this article:** Kang, D., Dai, J., Sun, H., Hou, Y. & Yuan, J. Quantum simulation of thermally-driven phase transition and oxygen *K*-edge x-ray absorption of high-pressure ice. *Sci. Rep.* **3**, 3272; DOI:10.1038/srep03272 (2013).